Interference effects with surface plasmons
Kuzmin, N.V.

CHAPTER 7

Short-wavelength surface plasmons

We report the generation and detection of surface plasmons propagating along a smooth buried silver/glass interface for incident wavelengths ranging from the blue well into the telecom band. Limited by ohmic loss, we reach photon energies of 2.6 eV, where the surface-plasmon wavelength equals 260 nm. These short-wavelength surface plasmons travel at one third of the speed of light in vacuo.

7.1   Introduction

Currently, there is considerable research activity in the field of plasmonics, one of the reasons being that surface plasmons provide a tool to structure light on a scale that is much finer than what can be achieved in free space or in a dielectric. A second goal of the research effort is to generate a form of slow light, allowing much enhanced interactions with resonant probes.

In the approach that is usually taken to achieve these goals the metallo-dielectric interface is *structured* either in the propagation direction, for instance by assembling an array of nano-sized metallic particles, or in the lateral direction, or both. On such a structured interface the surface plasmon is often quite rapidly damped as a consequence of radiative losses.

Alternatively, one can exploit the dispersion relation of a surface plasmon on an *unstructured* metallo-dielectric interface to generate short-wavelength (high-k), slow plasmons. Due to ohmic damping such high-k surface plasmons are either quite lossy or nonexistent, as is the case for gold. Here we explore the possibility of using a buried glass-silver interface for generating short-wavelength plasmons with a damping length of a few μm, more than sufficient for a variety of applications.

7.2   Dispersion and Damping

A surface plasmon is a solution to the wave equation that is bound to the interface between a dielectric, characterized by a real and positive relative permittivity ϵ_d, and a metal. The permittivity of the latter is always complex and is written as $\epsilon_m = \epsilon'_m + i\epsilon''_m$. At optical frequencies metallic behavior is associated with the requirement that $\epsilon'_m < 0$. Note that quite a few materials, such as tungsten and molybdenum, that are usually considered to be metallic do not fulfill this requirement over a considerable part of the optical spectrum.

For a surface plasmon to exist on a particular metallo-dielectric interface one must have $\epsilon'_m < -\epsilon_d < 0$. On a smooth interface its propagation constant is given by [8]:

$$k_{sp} = \frac{\omega}{c}\sqrt{\frac{\epsilon_m \epsilon_d}{\epsilon_m + \epsilon_d}}. \tag{7.1}$$

Since ϵ_m is a complex frequency-dependent quantity, so is k_{sp}. Hence we write:

$$k_{sp} = k' + ik'', \tag{7.2}$$

the imaginary part of k_{sp} quantifying the surface-plasmon damping length $L_{sp} = (k'')^{-1}$.

In the wavelength range where $\epsilon_m'' \ll -\epsilon_m'$ we can approximate the real and imaginary parts of k_{sp} as:

$$k' \simeq \frac{\omega}{c}\sqrt{\frac{\epsilon_m'\epsilon_d}{\epsilon_m' + \epsilon_d}}\,, \tag{7.3}$$

$$k'' \simeq \frac{\omega}{c}\frac{\epsilon_m''}{2\,(\epsilon_m')^2}\left(\frac{\epsilon_d\epsilon_m'}{\epsilon_d + \epsilon_m'}\right)^{3/2}. \tag{7.4}$$

In the appropriate wavelength interval the propagation constant k' of the surface plasmon can thus be well approximated by using Eq. (7.1) while neglecting the imaginary part of the permittivity [8]. Equation (7.4) shows that the real and imaginary parts of the wave vector of a surface plasmon are approximately related by:

$$\frac{k''}{k'} = \frac{\lambda_{sp}}{L_{sp}} \approx \frac{\epsilon_m''\epsilon_d}{2\,(\epsilon_m')^2}\left(\frac{k'}{\sqrt{\epsilon_d}k_0}\right)^2\,, \tag{7.5}$$

with $k_0 = \omega/c$. The factor in brackets, which is a measure for how much the surface-plasmon dispersion curve $\omega(k')$ deviates from the light line $\omega = ck_0/\sqrt{\epsilon_d}$, is of order unity. Consequently, the ratio of the imaginary and real parts of the surface-plasmon wave vector is approximately given by the quantity $\epsilon_d\epsilon_m''/2(\epsilon_m')^2$, which, for good metals, is much smaller than unity. The damping length of the surface plasmon $L_{sp} = (k'')^{-1}$, in units of the surface-plasmon wavelength $\lambda_{sp} = (k')^{-1}$, thus scales as ϵ_d^{-1}. From this perspective, the best dielectric is vacuum.

If, however, the aim is to reach small values of λ_{sp} it is advantageous to use a material that has $\epsilon_d > 1$. For instance, in the experiment described below we attain $\lambda_{sp} = 260$ nm using a silver-glass interface and 2.6 eV photons. The amplitude damping length of a 2.6 eV surface plasmon propagating along that interface equals $L_{sp} = 2$ μm. To achieve a similar value of λ_{sp} on a *silver-air interface* we require 3.5 eV photons, with $L_{sp} = 0.35$ μm. This counterintuitive result is caused by the strong dispersion of the dielectric permittivity of silver, particular at high photon energies.

7.3 Experiment

It is widely appreciated that films of gold and silver do not adhere well when deposited or sputtered on top of a glass surface. For that reason, it is quite common to first apply a bonding material, for instance a thin (nanometer-thick) layer of chromium or titanium (see Chapters 2–6). As compared to

gold and silver, both these metals are quite dissipative, and the bonding layer should be at most a few nm thick in order not to extinguish the surface plasmons on the glass-silver interface. In the present experiment we don't use such a dissipative adhesion layer.
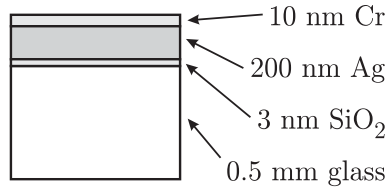

Figure 7.1. Structure of our sample.

In our samples, prepared by Laseroptik GmbH in Garbsen, Germany, we use a substrate made from borosilicate glass (Schott D263T), that is first coated with a 2–3 nm thick layer of *fused quartz* and, immediately after, with silver metal. Apparently, a freshly applied SiO_2 layer is sufficiently sticky to bind the Ag layer [124]. The silver film is 200 nm thick and is overcoated with a 10 nm thick layer of chromium. This top layer serves two purposes: to protect the silver film from becoming tarnished in ambient air, and to eliminate surface plasmons on the second interface [23]. A schematic of our film is shown in Fig. 7.1. The SiO_2 layer that sits between the glass and the silver is so thin that its presence is henceforth neglected. We have structured the silver film by means of ion-beam milling with a series of slit pairs, the two slits of a pair being separated by 8 or 25 μm, each slit being 100 nm wide and 50 μm long.

To measure the dispersion curve of the surface plasmon along the buried interface we use a so-called white-light laser (Fianium SC-450-2). This laser, when operated at full power ($\approx$ 2 W), emits a continuous spectrum spanning the wavelength region from 450 to 1700 nm. The output spectrum of the laser is reasonably flat (see Fig. 7.2) except for the region near $\lambda = 1064$ nm where the narrow-band seed laser emits. The polarization of the laser output shows no preferred axis.

By using a wedge beamsplitter, about 5% of the output of the laser is directed at our sample. It passes a polarizer mounted in a rotation mount so that the polarization of the light can be chosen. Subsequently, it impinges on the sample at normal incidence and the transmitted light is imaged on the entrance facet of a fiber spectrometer (Ocean Optics SD2000 for the visible part of the spectrum, and Ocean Optics NIR-512 for the near-infrared part). The polarization of the incident light is chosen to be TM (relative to the slits) so that surface plasmons can be excited on the buried interface.
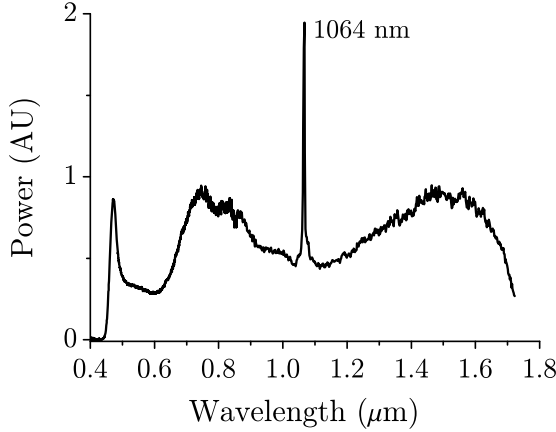
Figure 7.2. Spectrum of the Fianium SC-450-2 laser at full power. The experimental spectrum has been acquired by using a visible and IR fiber spectrometer and stitching the two data sets together.

In the present experiment the wavelength of the incident light spans nearly two octaves, from 450 to 1700 nm. Over this full range of incident wavelengths both the slit width and the film thickness are constant at a nominal value of 100 and 200 nm, respectively. The slit width thus varies between $\lambda/4$ and $\lambda/16$, the film thickness between $\approx \lambda/2$ and $\lambda/8$.

7.4 Results and Discussion

Figure 7.3 shows raw data for wavelengths between 400 and 1500 nm for an 8 μm and a 25 μm double slit. All spectra show a fast spectral modulation on top of a slowly varying spectrum. The latter represents the output of the Fianium laser as registered by our spectrometer, while the spectral modulation is due to plasmonic cross-talk as discussed in Chapter 2. While the modulation features are very well resolved in the near-infrared spectral region ($\lambda > 650$ nm) the visibility of the fringes rapidly decreases at shorter wavelengths. In the spectrum of the 8 μm double slit fringes can be seen down to wavelengths of 477 nm ($h\nu = 2.6$ eV); in contrast, for the 25 μm double slit the spectrum becomes featureless already at $\lambda = 530$ μm ($h\nu = 2.34$ eV). At long wavelengths ($\lambda > 1300$ nm), the spectral modulation vanishes also; at such small values of the wavelength-normalized slit width ($w/\lambda < 0.1$) the surface-plasmon excitation probability is predicted to become very small [35].

The features that we observe are due to interference: the light field that
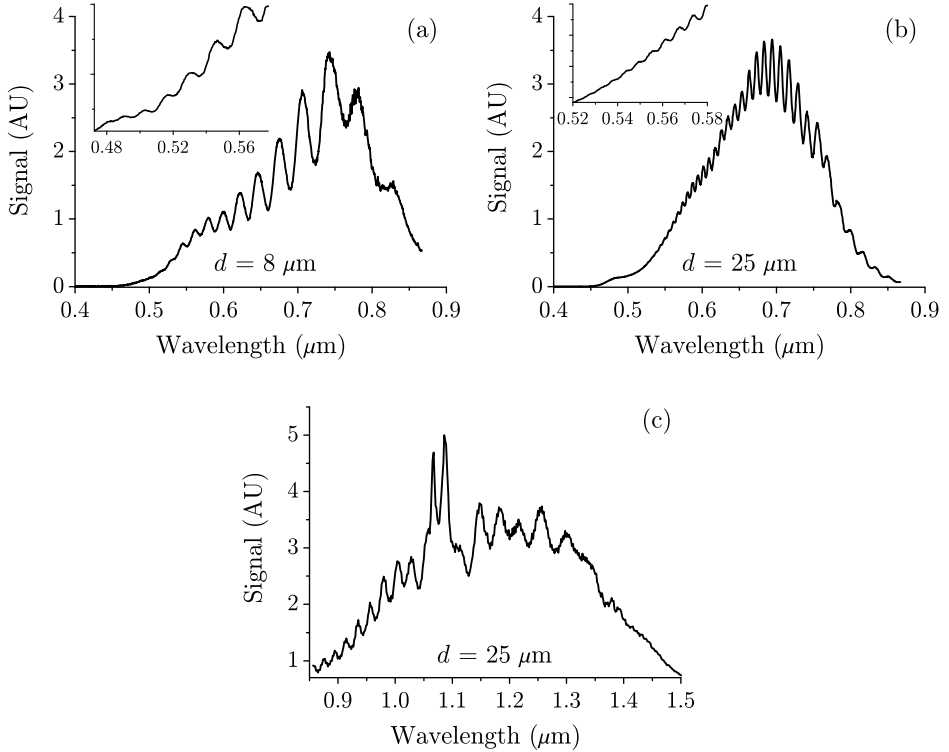
Figure 7.3. Uncorrected transmission spectra for a) an 8 μm double slit in the visible part of the spectrum, b) a 25 μm double slit, also in the visible part of the spectrum, and c) a 25 μm double slit in the IR part of the spectrum. The insets in a) and b) show a magnified view of the short-wavelength part of the spectra. The infrared spectrum carries a prominent doublet near $\lambda = 1.06$ μm, representing the strongly enhanced output of the laser near that wavelength, modulated by plasmonic cross-talk.

emanates from slit 1 is a coherent sum of (a small fraction of) the light field incident on that slit, and a small fraction of the field that falls on slit 2, is scattered into a surface plasmon that travels from slit 2 to slit 1 and is back-converted into a light field at slit 1. The amplitude of the field emanating from slit 1 can be written as:

$$E = E_0(\lambda)[1 + \alpha(\lambda)\cos(k'd + \pi)], \qquad (7.6)$$

where E_0 represents the amplitude of the field transmitted by slit 1, d is the distance between the slits and α a positive real coefficient describing the

scattering of light incident on slit 2, coupled into a surface plasmon, and re-radiated by slit 1. Both E_0 and α are explicitly dependent on the wavelength λ of the incident light. The phase factor π has been discussed in Chapter 5.

From the experimental spectra we can extract the wavelengths of the maxima and minima in the signal, the maxima corresponding to the case that $k'(\lambda)d = (2m+1)\pi$, while $k'(\lambda)d = 2m\pi$ at the minima. By a judicious choice of the value of m at a particular maximum or minimum we can associate values of m with all maxima and minima. Since we know d with sufficient accuracy we can extract values for the surface-plasmon propagation constant k' for all incident wavelengths. This allows us to construct a dispersion diagram of the surface plasmon (see Fig. 7.4).
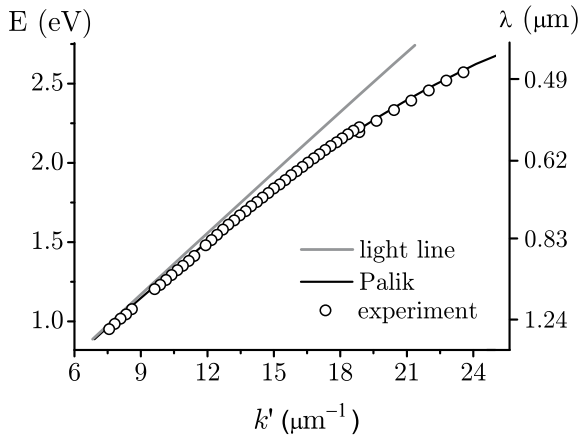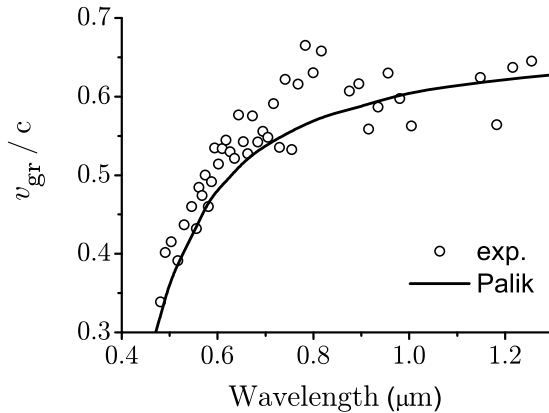

Figure 7.4. Dispersion curve for the surface plasmon along a smooth silver-glass interface. The circles give the experimental results, the black solid line the values of the real part of the surface-plasmon propagation constant calculated using Eq.(7.1) and the tabulated values for the dielectric permittivity of silver and the glass. The grey solid line shows the dispersion of a free electromagnetic wave propagating through the bulk glass.

The data points for $k' < 12 \ (\mu m)^{-1}$ have been recorded with the infrared spectrometer using the pair of slits separated by 25 μm; those for $18.6 \ (\mu m)^{-1} < k' < 12 \ (\mu m)^{-1}$ with the visible spectrometer and the 25 μm double slit, while those for $k' > 18.6 \ (\mu m)^{-1}$ were gathered with the 8 μm double slit. The solid line shows the dispersion curve according to Eq. (7.1), using the tabulated values for the dispersion of the real and imaginary parts of the refractive index of silver [22], and that of D263T borosilicate glass [125]. Finally, the grey solid line shows the dispersion of a free electromagnetic wave

through our glass with $n = 1.5166$ at $\lambda = 800$ nm. The experimental data are in excellent agreement with the calculated dispersion curve; to achieve this level of agreement we have to take the (small) dispersion of the refractive index of the D263T glass into account.

The last data point on our graph corresponds to a photon energy of 2.6 eV, i.e., a free-space wavelength of 477 nm. Using the tabulated values of the complex refractive index of silver we calculate the surface-plasmon damping coefficient for the silver-glass interface to be $k'' = 0.502$ $(\mu m)^{-1}$. Thus, the surface-plasmon (amplitude) damping length equals ≈ 2 μm, which explains why the modulation signal due to surface plasmons becomes very small for a slit separation of 8 μm, at these short wavelengths. The use of closer-lying slits (4 or 6 μm slit separation) did not allow us to measure plasmonic modulation at higher photon energies. Recently, Temnov *et al.* reported similar measurements on a bare (i.e., air-) silver interface; their experimental data terminated at $h\nu = 2.1$ eV, in the middle of the orange spectral region ($\lambda = 590$ nm) [73]. We conjecture that the difference is due to the superior quality and stability of our buried silver film. The use of a buried interface carries another advantage: at our highest-energy data point the surface-plasmon effective index $n_{sp} = c_0 k'/\omega = 1.83$, with c_0 the vacuum speed of light and ω the optical frequency. At this frequency we have $\lambda_{sp} = 260$ nm.


Figure 7.5. Dispersion of the group velocity of a surface plasmon along the buried quartz-silver interface. The data points are obtained by determining $\Delta\omega/\Delta k$ from adjacent experimental points in Fig. 7.4. The solid curve follows from the theoretical expression for the surface-plasmon dispersion (Eq. (7.1)).

From our data we can determine the dispersion of the surface-plasmon group

velocity on our interface (see Fig. 7.5). The scatter in the data represents the small deviations of the experimental data points away from the smooth dispersion curve of Fig. 7.4.

We observe the surface-plasmon group velocity to reach a value of $c_0/3$, with c_0 the vacuum speed of light, a reduction by a factor 2 as compared to surface plasmons in the infrared spectra region ($h\nu < 1.0$ eV). A similar reduction in surface-plasmon group velocity has recently been reported in a structured metallic waveguide [126].
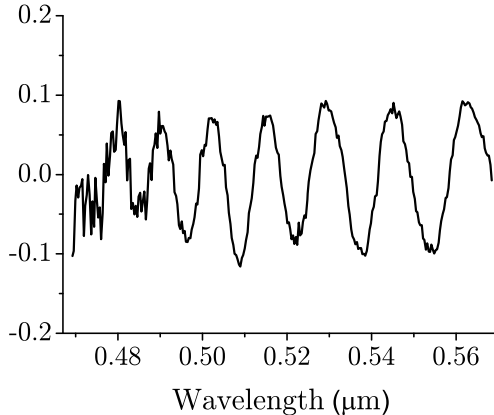
Figure 7.6. AC-component of the experimental data of Fig. 7.3 for the 8 μm double slit, corrected for the effect of surface-plasmon damping.

The spectra of Fig. 7.3 show that the spectral modulation varies considerably with the wavelength of the incident radiation, and that it is largest in the near-infrared spectral region. Various factors play a role here. First, we note that, according to Eq. (7.6), the modulation depth

$$M = 2 \frac{S(\lambda_{\max}) - S(\lambda_{\min})}{S(\lambda_{\max}) + S(\lambda_{\max})} \approx 4\alpha(\lambda) \tag{7.7}$$

provides a measure of the relative strength of the plasmonic and direct channels in the slit transmission. Therefore, the modulation depth is sensitive to factors that affect the direct channel, such as the ratio of slit width and incident wavelength, the ratio of slit depth and wavelength, *and* factors that affect the SP channel such as, again, the ratio of slit width and incident wavelength, and the surface plasmon damping along the interface. The latter effect can easily be calculated. In Fig. 7.6 we show the high-frequency component of the experimental data of the 8 μm double slit of Fig. 7.3, corrected for surface-plasmon damping using the dispersion data of Johnson and Christy [22]. The

corrected data show only a slight wavelength dependence, suggesting that the other factors play a minor role across the wavelength range covered in Fig. 7.6, or that these factors largely cancel each other.

7.5 Conclusions

We have performed a comprehensive study of the surface-plasmon dispersion on a glass-silver interface spanning 2 octaves in photon energy. Using a double-slit setup we have observed, up to photon energies of 2.6 eV, spectral features that are caused by an interference effect that involves a surface plasmon and light directly transmitted by the slits. At these high photon energies the surface plasmon on the silver-glass interface has a wavelength of only 260 nm and propagates with a group velocity equal to 1/3 of the speed of light in vacuum. Our experiments show that buried silver is an excellent and stable material for surface-plasmon studies and that the silver-glass interface gives access to surface plasmons with very short wavelengths.